THE JOURNAL OF BIOLOGICAL CHEMISTRY VOL. 288, NO. 40, pp. 28814–28823, October 4, 2013

Engraftment of a Galactose Receptor Footprint onto Adeno-associated Viral Capsids Improves Transduction Efficiency*

Received for publication, May 2, 2013, and in revised form, July 22, 2013 Published, JBC Papers in Press, August 12, 2013, DOI 10.1074/jbc.M113.482380

Shen Shen[‡§], Eric D. Horowitz[‡], Andrew N. Troupes[‡], Sarah M. Brown[‡], Nagesh Pulicherla[‡], Richard. J. Samulski[‡], Mavis Agbandje-McKenna[¶], and Aravind Asokan[‡§‖1]

From the [‡]Gene Therapy Center, [§]Department of Genetics, and [‖]Department of Biochemistry and Biophysics, University of North Carolina at Chapel Hill, Chapel Hill, North Carolina 27599 and the [¶]Department of Biochemistry and Molecular Biology, University of Florida, Gainesville, Florida 32610

Background: Viruses exploit cell surface glycans to infect host cells.
Results: Different adeno-associated viral serotypes were engineered to display functional galactose receptor footprints.
Conclusion: Chimeric, galactose-binding AAV strains display enhanced transduction efficiency while maintaining endogenous tissue tropism.
Significance: Grafting orthogonal glycan binding footprints onto AAV capsids can yield new chimeric strains with improved transduction profiles for therapeutic gene transfer applications.

New viral strains can be evolved to recognize different host glycans through mutagenesis and experimental adaptation. However, such mutants generally harbor amino acid changes that affect viral binding to a single class of carbohydrate receptors. We describe the rational design and synthesis of novel, chimeric adeno-associated virus (AAV) strains that exploit an orthogonal glycan receptor for transduction. A dual glycan-binding AAV strain was first engineered as proof of concept by grafting a galactose (Gal)-binding footprint from AAV serotype 9 onto the heparan sulfate-binding AAV serotype 2. The resulting chimera, AAV2G9, continues to bind heparin affinity columns but interchangeably exploits Gal and heparan sulfate receptors for infection, as evidenced by competitive inhibition assays with lectins, glycans, and parental AAV strains. Although remaining hepatotropic like AAV2, the AAV2G9 chimera mediates rapid onset and higher transgene expression in mice. Similarly, engraftment of the Gal footprint onto the laboratory-derived strain AAV2i8 yielded an enhanced AAV2i8G9 chimera. This new strain remains liver-detargeted like AAV2i8 while selectively transducing muscle tissues at high efficiency, comparable with AAV9. The AAV2i8G9 chimera is a promising vector candidate for targeted gene therapy of cardiac and musculoskeletal diseases. In addition to demonstrating the modularity of glycan receptor footprints on viral capsids, our approach provides design strategies to expand the AAV vector toolkit.

Virus-glycan interactions are critical determinants of host cell invasion. Cell surface carbohydrates such as sialic acids, gangliosides, or heparan sulfate are exploited by a vast number of viruses such as influenza, herpesvirus, SV40, polyomavirus, papillomavirus, and other pathogens (1, 2). In most cases, a single class of glycans primarily serves as the cell surface attachment factor for viruses, leading to sequential or parallel engagement of other receptors/coreceptors for cell entry. Adeno-associated viruses (AAVs)[2] are helper-dependent parvoviruses that exploit heparan sulfate (HS), galactose (Gal), or sialic acids (Sia) as primary receptors for cell surface binding (3, 4). For instance, AAV serotypes 2 and 3b utilize HS. AAV1, 4, and 5 bind Sia with different linkage specificities, whereas AAV9 exploits Gal for host cell attachment. Different AAV strains also require subsequent interaction with coreceptors such as integrin $\alpha V\beta 5$ or $\alpha 5\beta 1$, fibroblast growth factor receptor, platelet-derived growth factor receptor, EGF receptor, hepatocyte growth factor receptor, or the laminin receptor for cellular uptake (3, 4).

A notable exception to the monogamous relationship between a specific AAV strain and a single class of carbohydrates is AAV serotype 6, which recognizes both Sia and HS (5). However, only Sia has been shown to be essential for viral transduction. Structural studies have now established that the Lys-531 residue, in conjunction with Arg-488, Lys-528, and Lys-533 in the VP3 subunit of the AAV6 capsid, forms a continuous basic patch for electrostatic recognition of HS glycosaminoglycans (6–8). Similarly, the structural basis for HS recognition by AAV2 and AAV3b is well known and attributed to similar clusters of basic amino acid residues located at the 3-fold axis of symmetry (9–12). The Sia binding footprints for AAV1, AAV4, AAV5, and AAV6 remain to be determined. More recently, key amino acid residues involved in Gal recognition by AAV9 capsids were identified by using a combination of molecular modeling and site-directed mutagenesis (13).

* This work was supported, in whole or in part, by National Institutes of Health Grants R01HL089221 and P01HL112761 (to A. A. and R. J. S.), R01AI072176 (to R. J. S.), and R01GM082946 (to M. A. M.).
[1] To whom correspondence should be addressed: CB # 7352, Gene Therapy Center, 5123 Thurston Bldg., University of North Carolina, Chapel Hill, NC 27599-7352. Tel.: 919-843-7621; E-mail: aravind@med.unc.edu.

[2] The abbreviations used are: AAV, adeno-associated virus; HS, heparan sulfate; Gal, galactose; Sia, sialic acid; VP, viral protein; CBA, chicken β-actin; Luc, luciferase; vg, viral genome; qPCR, quantitative PCR; MOI, multiplicity/multiplicities of infection; ECL, *Erythrina crista-galli* lectin.

In this study, we exploited the abundance of structural information and knowledge pertaining to host receptor use by AAV serotypes to design a new class of chimeric glycan-binding AAV vectors for gene transfer applications. A new dual glycan-binding strain (AAV2G9) and a chimeric, muscle-tropic strain (AAV2i8G9) were generated by incorporating the Gal binding footprint from AAV9 into the AAV2 VP3 backbone or the chimeric AAV2i8 capsid template using structural alignment and site-directed mutagenesis. *In vitro* binding and transduction assays confirmed the exploitation of both HS and Gal receptors by AAV2G9 for cell entry. Subsequent *in vivo* characterization of the kinetics of transgene expression and vector genome biodistribution profiles indicate fast, sustained, and enhanced transgene expression by this rationally engineered chimeric AAV strain. A similar, improved transduction profile was observed with the liver-detargeted, muscle-specific AAV2i8G9 chimera. These new reagents provide a framework for exploiting the modularity of glycan receptor footprints to generate improved AAV vectors for gene transfer.

EXPERIMENTAL PROCEDURES

Structural Modeling—Coordinates for the AAV2 and AAV9 viral protein (VP) crystal structures were obtained from the RCSB Protein Data Bank (PDB codes 1LP3 and 3UX1, respectively) (14, 15). Using the SWISS-MODEL protein structure modeling server (16), homology models of the 2G9 and 2i8G9 VP3 monomers were generated with crystal structures of AAV2 VP3 as template. Three-dimensional icosahedral models of intact 2G9 and 2i8G9 capsids were created using the Oligomer Generator utility in VIPERdb-Virus Particle ExploreR2 (17). Similarly, illustration of the AAV2 VP3 trimer, 2i9 trimer, 2G9 trimer, 2i8G9 trimer, and AAV9 trimer were obtained using the Oligomer Generator utility. All structural models were visualized using PyMOL, with residues forming the galactose binding site (AAV9 VP1 numbering Asp-271, Asn-272, Tyr-446, Asn-470, Ala-472, Val-473, and Trp-503) (13) and heparan sulfate binding site (AAV2 VP1 numbering Arg-487, Lys-527, Lys-532, Arg-585, and Arg-588) (10–12, 18) highlighted in orange and purple, respectively. The i8 motif (AAV8 VP1 numbering 588-QQNTAP-593) was colored in deep blue (19). In VP3 trimer models, different monomers were colored in pale green, light blue, and light pink.

Generation of Dual Glycan-binding AAV Strains—The pXR2G9 chimera plasmid construct was generated by substituting amino acid residues directly involved and immediately flanking the Gal recognition site on the AAV9 VP3 capsid protein subunit onto corresponding residues on the VP3 subunit coding region of the helper plasmid pXR2 (AAV2 VP3 numbering Q464V, A467P, D469N, I470M, R471A, D472V, S474G, Y500F, and S501A). Substitutions were generated using the QuikChange Lightning site-directed mutagenesis kit (Agilent) using the following primers (IDT): 5′-GGAACCACCACGCAGTCAAGGCTTCA GTTTTCTGTGGCCGGACCCAGTAACATGGCTGTCCAGGGAAGGAACTGGCTTCCTGGACCCTGTTACCGC-3′ and 5′-GACATCTGCG GATAACAACAACAGTGAATTTGCTTGGACTGGAGCTACCAAGTACCACCT-3′. pXR2i8G9 was generated using the same set of primers to introduce amino acid substitutions at the same residues on the helper plasmid pXR2i8. Recombinant AAV vectors packaging the CBA-Luc transgene cassettes were generated as described previously, with modifications (20). Briefly, three plasmids were transfected into HEK293 cells: the AAV helper plasmid (pXR2, pXR2i8, pXR9, pXR2G9, or pXR2i8G9) encoding the *Rep2* and *Cap* genes, pXX6-80 containing the Adenoviral helper genes, and the pTR-CBA-Luc plasmid with the chicken β-actin (CBA) promoter-driven firefly luciferase (Luc) transgene flanked by inverted terminal repeats from the AAV2 genome. At 48–60 h post-transfection, cell pellets were collected, and pooled supernatants were subjected to PEG precipitation (8% w/v PEG8000, 0.5 M NaCl final concentration). Cell pellets and PEG precipitate were then pooled together prior to sonication and CsCl ultracentrifugation. Peak fractions containing the full viral particles were collected on the basis of refractive indices and infectivity of each fraction in HEK293 cells. After dialysis with 1× PBS overnight, viral titers were obtained by quantitative PCR using primers recognizing the luciferase transgene (5′-AAA AGC ACT CTG ATT GAC AAA TAC-3′ (forward) and 5′-CCT TCG CTT CAA AAA ATG GAA C-3′ (reverse)).

Heparin Affinity Chromatography—AAV2-CBA-Luc, AAV9-CBA-Luc, 2G9-CBA-Luc, 2i8-CBA-Luc, and 2i8G9-CBA-Luc were subjected to a heparin affinity column to assess their heparin-binding characteristics. 1e11 vg of AAV particles in 1 ml of 1× PBS buffer was loaded onto pre-equilibrated heparin affinity columns. After binding at room temperature for 30 min, viruses on the heparin column were eluted using 150 mM Tris buffer (pH 7.4) with an incrementally increasing concentration of NaCl (150 mM, 200 mM, 250 mM, 300 mM, 350 mM, 400 mM, 450 mM, 500 mM, 550 mM, 600 mM, 650 mM, 700 mM, and 750 mM). 1 ml of each individual eluate was collected and subjected to qPCR to quantify the total number of viral particles in each fraction. The percentage of loaded virions was calculated as the number of viral particles in eluate normalized by the total number of viral particles loaded onto the column.

In Vitro Binding and Transduction Assays—CHO-Pro5 and CHO-Lec2 cells were cultured in α minimum Eagle's medium (Thermo Scientific) supplemented with 10% FBS, 100 units/ml of penicillin (Cellgro), 100 μg/ml of streptomycin (Cellgro), and 2.5 μg/ml of amphotericin B (Sigma). Cells were seeded at a density of 1×10^5 cells/well in 24-well plates.

For competitive inhibition assays, CHO-Lec2 cells were prechilled at 4 °C for 30 min and incubated with 100 μg/ml of FITC-labeled *Erythrina crista-galli* lectin (FITC-ECL, Vector Laboratories) in α minimum Eagle's medium at 4 °C for 1 h. Alternatively, different viral capsids were incubated with 100 μg/ml of soluble heparin (Sigma) or 1× PBS (control) at room temperature for 1 h. Mock-treated or FITC-ECL-treated cells were then infected with HS-bound or mock-treated AAV2, AAV2G9, or AAV9 capsids packaging a CBA-Luc transgene cassette at an MOI of 1000 vg copies/cell. Following incubation in the cold room for 1 h, unbound virions were removed by three washes with ice-cold 1× PBS. For cell surface binding assays, the number of bound virions was measured by quantifying vector genome copy numbers/cell in each well using quantitative PCR. For transduction assays, infected Lec2 cells

were moved to 37 °C and incubated for 24 h prior to quantitation of luciferase transgene expression from cell lysates.

Competitive Inhibition Assays with Parental AAV Strains—Parental AAV2, AAV9, or 2i8 vectors packaging a CBA promoter-driven tdTomato transgene cassette were utilized as competitors for transduction. Briefly, Lec2 cells were seeded in 24-well plates overnight at a density of 1×10^5 cells/well. After being prechilled at 4 °C for 30 min, Lec2 cells were preincubated with either AAV2-tdTomato, 2i8-tdTomato, or AAV9-tdTomato vectors at multiplicities of infection ranging from 500–100,000 vg/cell at 4 °C for another 30 min. Cells were then superinfected with AAV2G9-CBA-Luc or AAV2i8G9-CBA-Luc at an MOI of 1000 vg/cell for 45 min at 4 °C, followed by removal of unbound virions using ice-cold PBS. Infected cells were then incubated at 37 °C for 24 h prior to luciferase expression analysis. The luciferase activity shown in relative light units indicates the transduction efficiency of the AAV2G9-CBA-Luc or AAV2i8G9-CBA-Luc vectors.

In Vitro Transduction Assays—To compare the *in vitro* transduction efficiency of Gal-binding chimeric strains with the parental strains, AAV2i8, AAV2i8G9, and AAV9 packaging the CBA-Luciferase transgene were added to prechilled Pro5 or Lec2 cell cultures at an MOI of 1000 vg/cell. After incubation at 4 °C for 1 h, unbound virions were removed by three washes with ice-cold 1× PBS, and fresh medium was added to the Pro5 and Lec2 cultures. 18–24 h post-transduction, cells were lysed to quantify the expression efficiency of the luciferase transgene.

Kinetics of Transgene Expression in Vivo—Female BALB/c mice (6–8 weeks old) were purchased from Jackson Laboratories and handled in accordance with National Institutes of Health guidelines using Institutional Animal Care and Use Committee-approved protocols at the University of North Carolina Chapel Hill. Different AAV vectors packaging the CBA-Luc cassette were injected intravenously into the tail vein at a dose of 1×10^{11} vg/mouse. At the indicated time intervals post-administration (3, 7, and 18 days), mice were injected intraperitoneally with luciferin (120 mg/kg, Nanolight), and bioluminescent images were obtained using a Xenogen IVIS® Lumina system (Caliper Lifesciences). Quantitation of light output from liver and whole animal images was carried out using IgorPro® software (Wavemetrics). Further quantitation of luciferase transgene expression and vector genome biodistribution in different tissues was carried out in two different groups of mice that were sacrificed at days 3 and 18 post-vector administration. Luciferase transgene expression was monitored in different tissue lysates as described earlier. Vector genome biodistribution was determined by first extracting genomic DNA from tissue lysates using a DNeasy® kit (Qiagen). The luciferase transgene copy number was determined using qPCR and normalized to DNA concentration. Primers 5′-AAAAGCACTCTGATTGACAAATA C-3′ and 5′-CCTTCGCTTCAAAAAATG GAAC-3′ were used to quantify CBA-Luciferase transgene copy number by qPCR.

Statistical Analysis—All data are expressed as mean ± S.E., and the number of replicates for each experiment is provided in the corresponding figure legends. Statistical significance was determined using unpaired one-tail Student's *t* test, and $p <$ 0.05 was considered statistically significant for different experiments unless indicated otherwise.

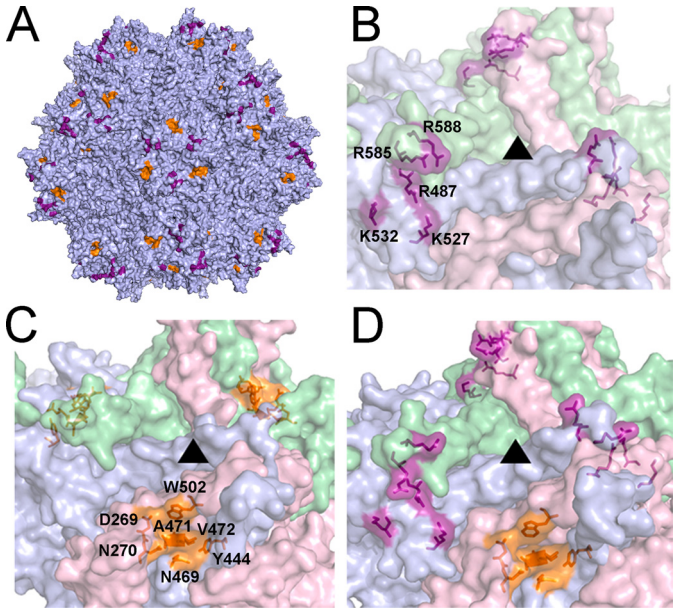

FIGURE 1. **Three-dimensional models of the dual glycan-binding AAV2G9 chimera and its parental strains AAV2 and AAV9.** *A*, three-dimensional structural model of an intact AAV2G9 capsid with existing HS and "grafted" Gal binding residues shown in *purple* and *orange*, respectively. *B–D*, illustrations of the three-dimensional surface models of VP3 trimers at the 3-fold symmetry axes of AAV2 (*B*), AAV9 (*C*), and AAV2G9 (*D*) capsids. ▲ indicate the 3-fold axes of symmetry. Residues involved in HS binding (AAV2 VP1 numbering Arg-487, Lys-527, Lys-532, Arg-585, and Arg-588) and Gal binding (AAV9 VP1 numbering Asp-271, Asn-272, Tyr-446, Asn-470, Ala-472, Val-473, and Trp-503) are highlighted as in *A*.

RESULTS

Construction of a Novel, Dual Glycan-binding AAV Strain—To explore the feasibility of "grafting" the Gal footprint of AAV9 onto several AAV strains, we first compared the three-dimensional structures of the VP3 subunit trimers of AAV serotypes 1, 2, 6, and 8 in alignment with that of AAV9. Amino acid residues on the template capsids that overlapped with corresponding AAV9 VP3 residues directly involved in binding or immediately flanking the Gal receptor footprint were modified by multiple rounds of site-directed mutagenesis. The chimeric AAV strains generated were prepared as recombinant vectors packaging a chicken β-actin promoter-driven firefly luciferase (CBA-Luc) reporter transgene cassette using protocols established previously (20). Amino acid residues involved in Gal recognition and other flanking residues from AAV9 were remarkably well tolerated on different AAV serotype capsids because the packaging efficiencies of these AAV chimeras are comparable with parental strains. Multiple AAV chimeras on the basis of AAV serotypes 1, 2, 6, and 8 and the previously engineered AAV2i8 mutant (19) were obtained (at titers ranging from 5×10^{11} to 5×10^{12} viral genome copies/ml, data not shown). We first carried out a detailed characterization of the dual glycan-binding AAV chimera, dubbed AAV2G9 (where "g" stands for the Gal footprint and the numbers identify the recipient and donor capsid serotypes, respectively).

Three-dimensional models of the engineered AAV2G9 (full capsid in Fig. 1*A* and VP3 trimer in *D*) with the putative dual

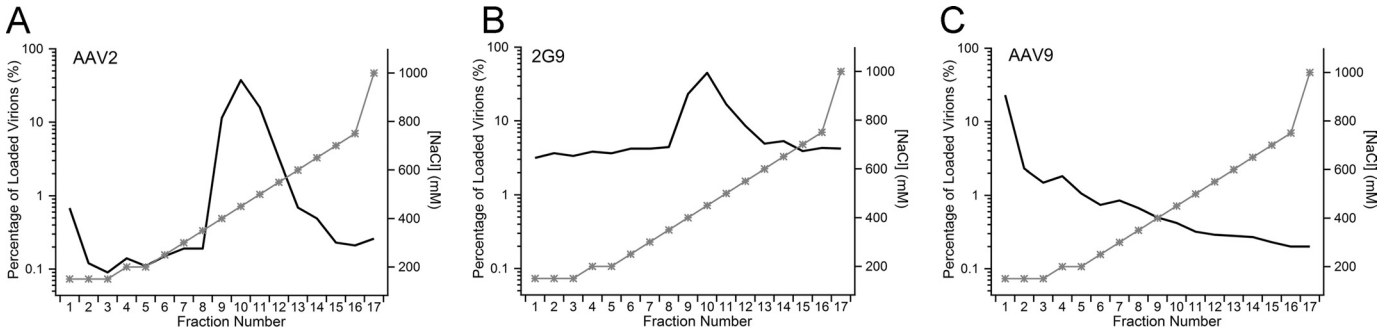

FIGURE 2. **Heparin binding characteristics of AAV2, AAV2G9, and AAV9.** *A*, heparin affinity column chromatogram of parental AAV2 vectors. A total of 1e11 vg containing particles of AAV2-CBA-Luc in 1 ml of 1× PBS was loaded onto a heparin affinity column. Bound virions were eluted from the heparin affinity column by elution with increasing NaCl concentration (*right y axes*, *gray lines*). The numbers of vg in the loaded sample and each eluted fraction were quantified using qPCR as described under "Experimental Procedures." The numbers of vg in each fraction were normalized to the total loaded vg to obtain the percentage of recovered virions (*left y axes*, *black lines*). Heparin affinity column chromatograms of AAV2G9 (*B*) and AAV9 (*C*) were obtained through a similar approach.

glycan receptor binding sites (HS and Gal) highlighted in *purple* and *orange* were generated by homology modeling using SWISS MODEL (Basel, Switzerland). The molecular model of AAV2G9 full capsids demonstrates the geometrical distribution and orthogonality of HS and Gal binding sites located around the 3-fold symmetry axis on the icosahedral capsid. Close-up views of HS and Gal receptor footprints from the 3-fold axes further support the observation that grafting orthogonal Gal binding sites on the backbone of the AAV2 capsid can be tolerated with regard to capsid assembly. Three-dimensional structures of the AAV2 VP3 subunit trimer with side chains of positively charged residues involved in HS recognition (highlighted in *purple*, Fig. 1*B*) as well as the side chains of amino acid residues comprising the Gal recognition site on the AAV9 VP3 subunit trimer (highlighted in *orange*, *C*) are also shown. The key residues involved in HS binding by AAV2 (VP1 numbering Arg-487, Lys-527, Lys-532, Arg-585, and Arg-588; *boldface* and *underlined*) are distinct from previously identified Gal binding residues on AAV9 (VP1 numbering Asp-271, Asn-272, Tyr-446, Asn-470, Ala-472, Val-473, and Trp-503; *black arrowheads*). Both key amino acids as well as flanking residues were mutated (AAV2 VP1 numbering Q464V, A467P, D469N, I470M, R471A, D472V, S474G, Y500F, and S501A; *white font*, highlighted in *black*) to graft the three-dimensional Gal-binding footprint onto the AAV2 template.

The Engrafted Gal Footprint Is Functionally Orthogonal to the HS Footprint on the AAV2 Capsid—On the AAV2G9 capsid surface, the HS and Gal footprints are composed of distinct amino acids (Fig. 1). Engraftment of the Gal footprint did not change the packaging capacity of AAV2G9 compared with the parental AAV2, as indicated by similar titers of viral preparations, supporting the structural compatibility of the Gal footprint with AAV2 capsid architecture. To probe for the impact of Gal footprints on the global conformation and functionality of AAV2 capsids, heparin affinity column chromatography was carried out with AAV2G9 and the two parental strains, AAV2 and AAV9 (Fig. 2). In the case of AAV2 (Fig. 1*A*), viral particles were eluted from the heparin affinity column in peak fractions at a concentration of 450 mM saline, consistent with previous publications (6, 21). In contrast, the Gal-binding AAV9 was found primarily in flow-through fractions at concentrations as low as 150–200 mM, indicating a low affinity for HS (Fig. 2*C*). The chimeric AAV2G9 demonstrates HS-binding properties similar to that of AAV2 (Fig. 2*B*), with chimeric particles eluting at a concentration of 450 mM saline. These results suggest that the engraftment of a Gal binding footprint onto the AAV2 capsid does not alter the heparin-binding characteristics of AAV2.

AAV2G9 Exploits HS and Gal Receptors Interchangeably in Vitro—The first line of evidence supporting the usage of dual glycan receptors by AAV2G9 was obtained from competitive inhibition assays of virus binding on the cell surface involving soluble heparin and ECL, which selectively binds terminally galactosylated glycans. A mutant CHO cell line, CHO-Lec2, is deficient in transporting CMP-sialic acids from Golgi compartments to the cell surface (22). Therefore, the majority of terminal glycan moieties on the CHO-Lec2 surface are galactose. This unique galactosylation pattern on the surface of CHO-Lec2 and sialylation of wild-type CHO-Pro5 cells can be useful in studying AAV-galactose/AAV-sialic acid interactions (23, 24). As seen in Fig. 3, *A* and *C*, HS, but not ECL, significantly inhibits AAV2 transduction in CHO-Lec2 cells (*dark gray bars*), whereas ECL selectively blocks AAV9 transduction by nearly two log units (*white bars*). These results are consistent with the expected transduction profiles for AAV2 and AAV9 (24–26). In contrast, AAV2G9 can only be effectively neutralized by pretreatment with a combination of both ECL and HS (*light gray bars*, Fig. 3*B*). A small but significant inhibitory effect is observed for ECL.

The transduction profiles for AAV2, AAV9, and AAV2G9 were further corroborated by inhibition of cell surface binding of each strain using ECL or HS (Fig. 3, *D*–*F*). The unique cell surface attachment of the chimeric AAV strain is further supported by competitive inhibition of cell surface attachment of AAV2G9 exclusively by a combination of ECL and HS but neither reagent alone (Fig. 3*E*). Such a scenario can be expected on the basis of the apparent ability of AAV2G9 to bind two different glycans interchangeably.

AAV2G9 Mediates Rapid Onset of Transgene Expression in Vivo—We then investigated whether the orthogonal Gal footprint confers specific advantages to AAV2G9 transduction *in vivo*. Live animal imaging studies were carried out to monitor luciferase transgene expression following systemic administration of different AAV strains in BALB/c mice. Bioluminescent

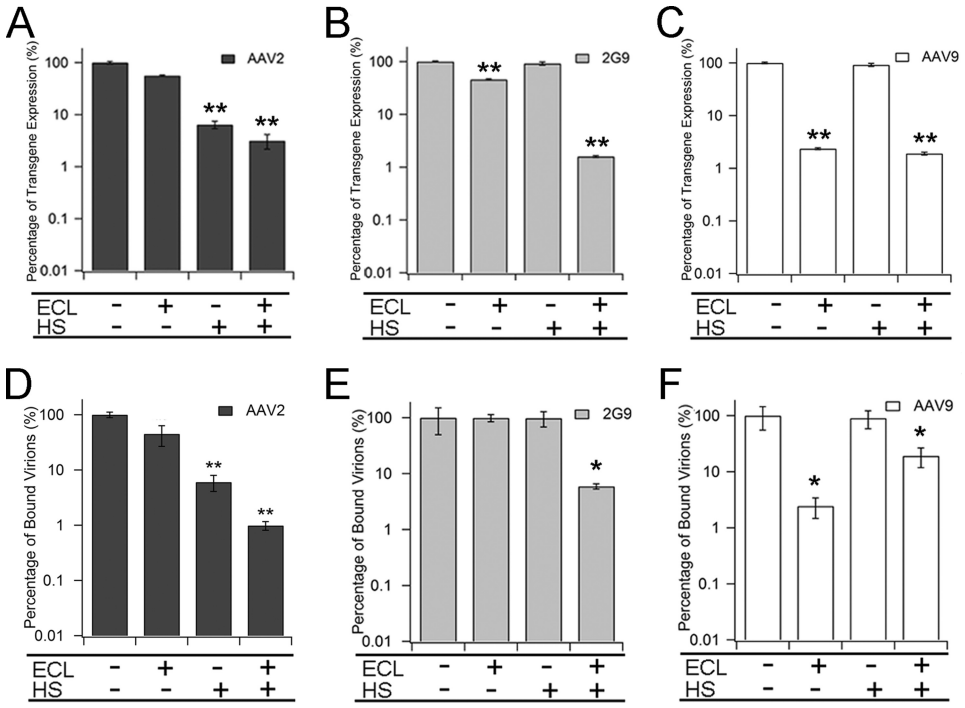

FIGURE 3. ***In vitro* characterization of the dual glycan-binding AAV2G9 chimera.** *A–C*, inhibition of AAV2 (*A*), AAV2G9 (*B*), and AAV9 (*C*) transduction on CHO Lec2 cells with FITC-ECL and soluble heparin. CHO Lec2 cells were prechilled at 4 °C and incubated with FITC-ECL, soluble heparin, or both prior to infection with AAV2, AAV2G9, or AAV9 packaging a CBA-luciferase reporter transgene cassette. Transduction efficiency was measured 24 h post-infection as luciferase activity in relative light units. The percentage of transgene expression was calculated by normalizing transduction efficiency to relative light units from controls. Results are presented as mean ± S.E. ($n = 4$). *D–F*, inhibition of cell surface binding of AAV2 (*D*), AAV2G9 (*E*), and AAV9 (*F*) on CHO Lec2 cells with FITC-ECL and soluble heparin. Different AAV particles were bound to cells prechilled at 4 °C, and unbound virions were removed by washing with cold PBS. Bound virions were quantified using qPCR after viral genome extraction. The percentage of bound virions was determined by normalizing number of bound virions to that of corresponding controls. Results are presented as mean ± S.E. ($n = 5$). Statistical significance was analyzed using one-tailed Student's *t* test. *, $p < 0.05$; **, $p < 0.01$.

images (Fig. 4*A*) and quantitative assessment of light output within the liver (*B*) and the whole animal (*C*) obtained at days 3, 7, and 18 post-injection support the notion that AAV2G9 can mediate rapid onset and enhanced gene expression. As shown in Fig. 4*A*, the kinetic profile displayed by AAV2G9 mirrors that of AAV9 but not AAV2. Further, the transduction profile/tissue tropism of AAV2G9 appears to be primarily hepatotropic, similar to AAV2 and, unlike the systemic tropism displayed by AAV9, as established previously (4, 27–29). Quantitation of the kinetics of bioluminescent signal output (Figs. 4, *B* and *C*) suggests that the transduction efficiency of AAV2G9 is enhanced in multiple organs. Notably, the efficiency and onset of liver transduction by AAV2G9 is comparable with that of AAV9, as quantified from live-animal images (Fig. 4*B*). Thus, dual glycan receptor engagement appears to improve the transduction efficiency and expedite the onset of transgene expression by this chimeric AAV strain without altering tissue tropism.

To further evaluate the *in vivo* transduction profile of AAV2G9, a quantitative analysis of tissue lysates from BALB/c mice were carried out at 18 days post-administration. Specifically, the transduction efficiency of AAV2G9 in the brain, lung, and spleen remains similar to that of AAV2 at 18 days post-intravenous administration. Interestingly, AAV2G9 displays a significantly higher luciferase transgene expression in the heart (~25-fold increase), liver (~4-fold increase), skeletal muscle (~4-fold increase), and kidney (~4-fold increase) compared with the AAV2-treated group. Importantly, the transduction efficiency of AAV2G9 in the liver is comparable with AAV9 (less than a 5-fold difference). These results support a potential role for the orthogonal Gal receptor that might involve the creation of an alternative tissue uptake pathway(s). The latter attribute could account for the uniform, multiorgan improvement in the transduction profile of AAV2G9.

Construction of AAV2i8G9, an Artificial Gal-binding AAV Strain—To further scrutinize the modularity and functionality of the Gal binding footprint, the HS binding capacity of AAV2G9 was abrogated by mutating the partial HS binding linear motif (585-RGNRQA-590) to the corresponding motif from AAV8 (585-QQNTAP-590). The resulting chimera, AAV2i8G9, was thus constructed on the basis of an AAV2i8 chimera (19), thereby enabling studies solely focused on the Gal motif in the AAV2 capsid context. The original AAV2i8 chimera has been described by our laboratory earlier (19). As shown in Fig. 5, *A* and *B*, there is no overlapping amino acid between the "I" motif from AAV8 (*deep blue*, AAV2i8G9 VP1 numbering 585-QQNTAP-590) and the "G" motif from AAV9 (*orange*; AAV2i8G9 VP1 numbering V464, P467, N469, M470, A471, V472, G474, F500, and A501). The yield of AAV2i8G9 viral particles is similar to that of the parental strains of AAV2 and AAV9. This observation supports the notion that the latter motifs are compatible with each other on an AAV2 capsid template. Consistent with earlier studies (19), AAV2i8 is unable to bind to HS, as shown by heparin affinity column chromatography (Fig. 5*C*). Incorporation of a Gal footprint does not appear

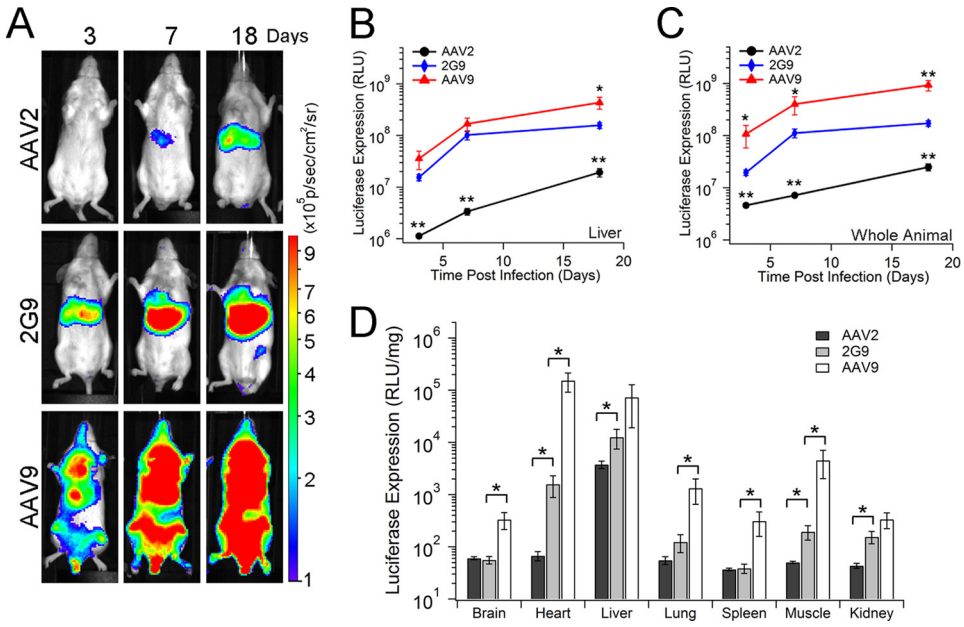

FIGURE 4. **AAV2G9 mediates rapid onset and enhanced transgene expression *in vivo*.** *A*, *in vivo* transgene expression kinetics of AAV2, AAV2G9, and AAV9 vectors packaging a CBA-luciferase transgene cassette. BALB/c mice ($n = 4$) were administered AAV vectors at a dose of 1×10^{11} vg/animal through the tail vein, and bioluminescent images were collected at 3, 7, and 18 days post-injection using an Xenogen® Lumina imaging system. Representative live animal images are shown with bioluminescence on a rainbow-colored scale (1×10^5-1×10^6 photons/second/cm^2/steradian). AAV2G9 maintains the hepatic tropism of AAV2 but demonstrates a more rapid and robust luciferase signal than both parental AAV strains. *B* and *C*, quantitation of the kinetics of light signal output (expressed as photons/second/cm^2/steradian) was performed by marking regions of interest around images of the liver regions (*B*) and entire animals (*C*) obtained at different time intervals ($n = 4$). *RLU*, relative light unit. *D*, quantitation of luciferase transgene expression in major tissues from AAV2- (*black*), AAV2G9- (*gray*), or AAV9-treated (*white*) animals at 18 days post-administration ($n = 4$). BALB/c mice ($n = 4$) were administered AAV2, AAV2G9, or AAV9 packaging a CBA-Luciferase cassette at a dose of 1×10^{11} vg/animal through the tail vein. At 18 days post-vector administration, animals were sacrificed to harvest brain, heart, liver, lung, spleen, skeletal muscle, and kidney tissues. Luciferase transgene expression in these tissue lysates was measured using a luminometer and normalized by the total amount of protein in each sample, determined using a Bradford assay. Statistical significance was assessed using one-tailed Student's *t* test. *, $p < 0.05$; **, $p < 0.01$.

to affect the inability of the AAV2i8G9 to bind to the heparin affinity column (Fig. 5*D*). Both chimeric strains were essentially obtained in eluate fractions.

To further interrogate the exploitation of alternate transduction pathways by introducing the Gal motif, we conducted competition assays of AAV2G9 and AAV2i8G9 with their corresponding parental serotypes. As shown in Fig. 6*A*, preincubation with competing vectors AAV2-CBA-tdTom (*solid line*, ●) or AAV9-CBA-tdTom (*dotted line*, ▲) at MOIs ranging from 500 to 100,000 vg/cell does not efficiently block transduction in CHO-Lec2 cells by AAV2G9-CBA-Luc, as measured by luciferase transgene expression at 24 h post-transduction. Only mild inhibitory effects were visible at 10-fold MOI of AAV2-tdTom (~10%) or AAV9-tdTom (~10%). At higher MOI (100-fold excess), AAV2 appears to compete less effectively (~30% inhibition) than AAV9 (~60% inhibition) by neutralizing AAV2G9 transduction. Taken together, these results support the notion that AAV2G9 is indeed a novel, dual glycan-binding strain with the unique ability to exploit both HS and Gal interchangeably as primary receptors for transduction.

A similar competitive inhibition assay was carried out with AAV2i8G9 (Fig. 6*B*). At MOI of the competing AAV2i8-tdTom ranging from 500–100,000 vg/cell, the transduction efficiency of AAV2i8G9 on CHO-Lec2 cells was not affected significantly compared with control Lec2 cells transduced with AAV2i8G9-CBA-Luc vectors alone. This observation is consistent with the inability of both AAV2i8 and AAV2i8G9 to bind HS on the cell surface. In contrast, in the presence of competing AAV9-tdTom, which binds Gal, transduction of Lec2 cells by AAV2i8G9 is blocked efficiently. With an equal MOI of AAV9-tdTom and AAV2i8G9-CBA-Luc present, only 48% of the Lec2 cells were transduced by AAV2i8G9 compared with the control. When there was a 10-fold excess of AAV9-tdTom competitors present, the transduction efficiency of AAV2i8G9 was blocked by ~80%. At 100-fold excess, AAV9-tdTom ~93% inhibition of AAV2i8G9 transduction was observed. These results support the notion that AAV2i8G9 utilizes Gal as the primary glycan receptor for cell surface attachment and entry.

In Vitro and in Vivo Transduction Profiles of AAV2i8G9—The *in vitro* characterization of AAV2i8G9 was carried out on CHO-Pro5 and CHO-Lec2 cells with its parental controls, AAV2i8 and AAV9 (Fig. 7*B*). *In vitro* transduction assays indicate that AAV2i8G9 transduces CHO-Lec2 cells as efficiently as AAV9, supporting the notion that Gal is a primary receptor for this chimeric strain. The transduction efficiency of AAV2i8G9 on CHO-Lec2 is ~3 orders of magnitude higher than that on CHO-Pro5 because of the abundance of terminal galactose on the CHO-Lec2 cell surface. Similar trends have been reported for AAV9, which binds to galactose on the CHO-Lec2 cell surface (24, 26). A modest increase in transduction efficiency of AAV2i8G9 compared with AAV2i8 on CHO-Pro5 was noted, most likely because of interactions with residual terminal galactose residues on CHO-Pro5.

The *in vivo* transduction profiles of AAV2i8G9 were obtained at days 3, 7, and 18 post-intravenous administration in BALB/c mice (Fig. 7*A*). As reported earlier by our group,

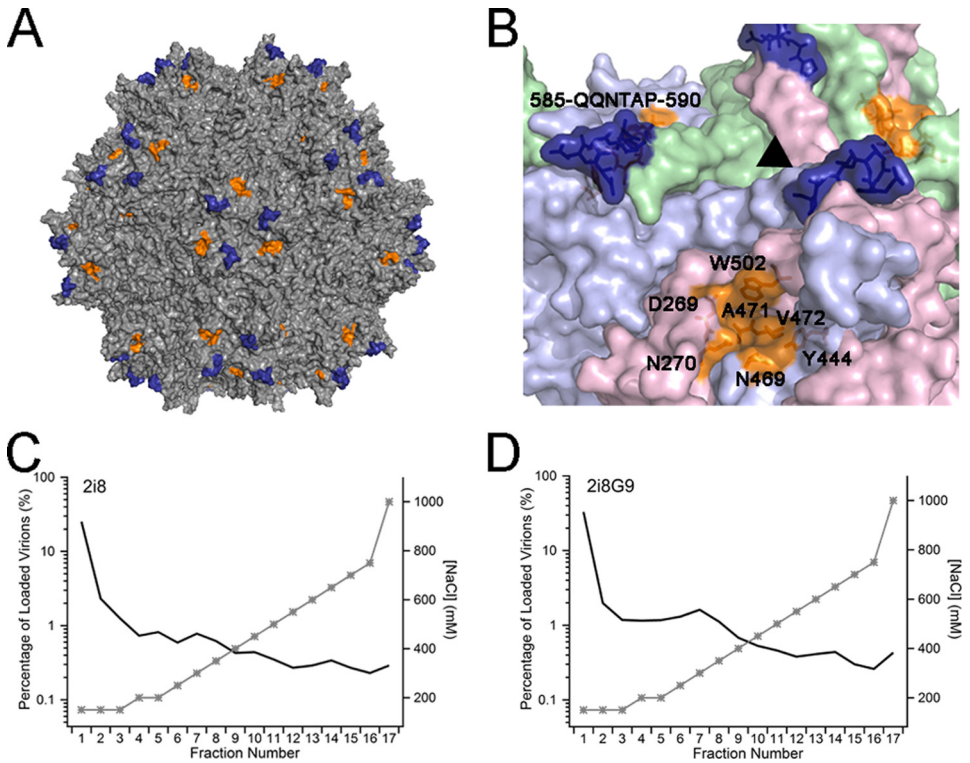

FIGURE 5. **Structural attributes of the AAV2i8G9 chimera.** *A*, three-dimensional illustration of the intact AAV2i8G9 capsid. The surface-exposed motif derived from AAV8 (AAV8 VP1 numbering 588-QQNTAP-593) and the Gal binding site from AAV9 (AAV9 VP1 numbering Asp-271, Asn-272, Tyr-446, Asn-470, Ala-472, Val-473, and Trp-503) are shown in *deep blue* and *orange*, respectively. *B*, close-up view of the 3-fold axes of symmetry (▲) on the exterior of the AAV2i8G9 capsid. Three individual VP3 monomers are shown in *pale green*, *light blue*, and *pale pink*. The structural motifs derived from the AAV8 and AAV9 motifs are highlighted as described in *A*. *C* and *D*, heparin affinity column chromatograms of the parental AAV2i8 strain (*C*) and the AAV2i8G9 chimera (*D*). A total of 1e11 vg of AAV2i8 or AAV2i8G9 vectors in 1 ml of 1× PBS were loaded onto heparin affinity columns. Virions were eluted from the column with elution buffers containing increasing concentrations of NaCl (*right y axes*, *gray lines*). The percentage of recovered virions in each elution fraction (*left y axes*, *black lines*) was obtained by normalizing the total number of vg in each fraction to that in the loaded sample.

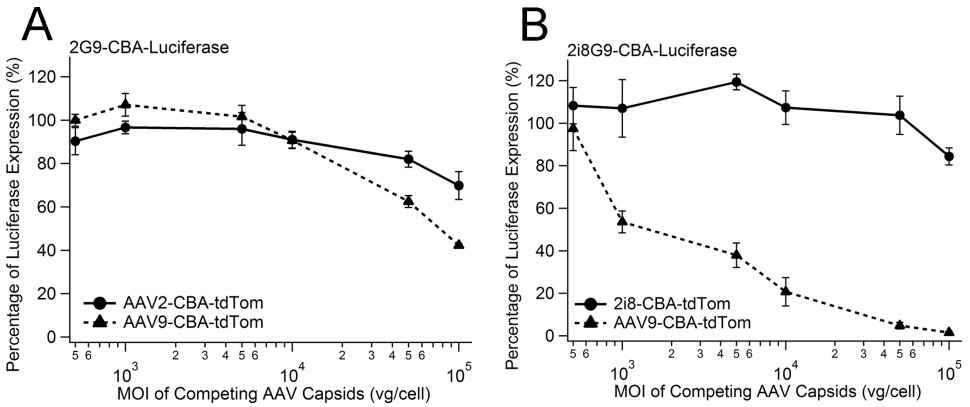

FIGURE 6. **Competitive inhibition of AAV2G9 and AAV2i8G9 by parental AAV serotypes.** *A*, CHO Lec2 cells were preincubated with AAV2 or AAV9-CBA-tdTomato at MOI ranging from 500–100,000 vg/cell for 2 h. Pretreated cells were then infected with AAV2G9-CBA-Luc particles (MOI = 1000 vg/cell). At 24 h post-transduction, cells were lysed to assess luciferase activity. Percentage inhibition of AAV2G9 transduction was calculated by normalizing luciferase transgene expression levels to that of control with no AAV competitors. *B*, competitive inhibition of AAV2i8G9-CBA-Luc transduction by AAV2i8-tdTomato and AAV9-tdTomato was carried out in a similar fashion. The percentage of luciferase expression was obtained by normalizing the luciferase transgene expression in each condition by that of the control condition without any competitor AAV. Results are presented as mean ± S.E. ($n = 4$). Statistical significance was analyzed using one-tailed Student's *t* test. *, $p < 0.05$; **, $p < 0.01$.

AAV2i8 is detargeted from the liver and demonstrates selective tropism for cardiac and skeletal muscle (19). As shown in live animal images, AAV2i8G9 retains a liver-detargeted transduction profile similar to that of AAV2i8. Notably, the kinetics of transgene expression mediated by AAV2i8G9 in the entire animal are comparable with those of AAV9 and more rapid than AAV2i8 (Fig. 7*C*). Luciferase expression levels in tissue lysates from BALB/c mice at 18 days post-administration further corroborate these observations (Fig. 7*D*). In murine heart, liver, lung, and kidney tissues, AAV2i8G9 shows a transduction efficiency in between that of AAV2i8 and AAV9. Importantly, transgene expression mediated by AAV2i8G9 in the liver is only ~5-fold higher than that of AAV2i8 but remains nearly 200-fold less than that of AAV9. In addition, AAV2i8G9 demonstrates a modestly higher efficiency when compared with either AAV2i8 or AAV9 in skeletal muscle. Taken together, these observations con-

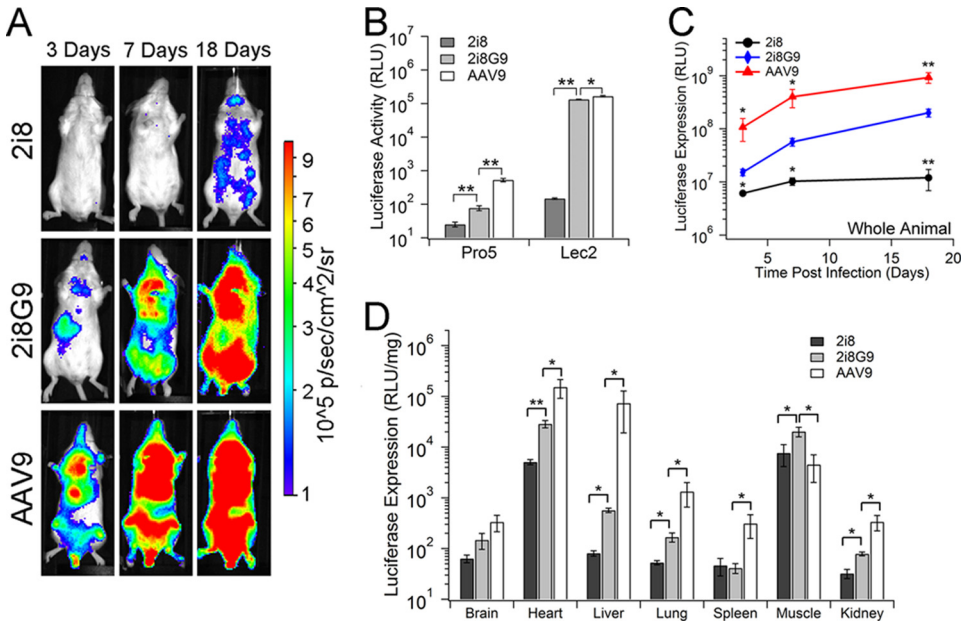

FIGURE 7. **AAV2i8G9 demonstrates an enhanced and selective transduction profile in skeletal muscle.** *A*, *in vivo* transgene expression kinetics of AAV2i8, AAV2i8G9, and AAV9 vectors packaging the CBA-luciferase transgene cassette. BALB/c mice ($n = 4$) were administered AAV2i8, AAV2i8G9, and AAV9 vectors at a dose of 1×10^{11} vg/animal through the tail vein. Live animal bioluminescent images were collected at 3, 7, and 18 days post-injection using an Xenogen® Lumina imaging system. Representative live animal images are shown on a rainbow-colored scale (1×10^5-1×10^6 photons/second/cm^2/steradian). *B*, *in vitro* transduction efficiency of AAV2i8, AAV2i8G9, and AAV9 on CHO-Pro5 and Lec2. Vectors packaging CBA-luciferase were bound to prechilled Pro5 or Lec2 at an MOI of 1000 vg/cell at 4 °C for 1 h. Unbound virions were removed by three washes with ice-cold 1× PBS, and luciferase transgene expression was measured at 18–24 h post-infection. Results are shown in relative light units (*RLU*) ($n = 5$). Statistical significance was analyzed using one-tailed Student's *t* test. *, $p < 0.05$; **, $p < 0.01$. *C*, quantitation of the kinetics of transgene expression by AAV2i8, AAV2i8G9, and AAV9 in BALB/c mice. Regions of interest were marked around the entire animals in live-animal images (*A*) to measure the light signal output (expressed as photons/second/cm^2/steradian) from the mice at different time intervals ($n = 4$). Statistical significance was assessed to compare AAV2i8 and AAV2i8G9 as well as AAV9 and AAV2i8G9. *D*, *in vivo* transduction efficiency of AAV2i8, AAV2i8G9, and AAV9 in BALB/c mice. At 18 days post-administration, animals were sacrificed, and luciferase transgene expression in tissue lysates from brain, heart, liver, lung, spleen, muscle, and kidney were determined using a luminometer. Results are normalized to the amount of protein in each sample measured by Bradford Assay and presented as mean ± S.E. ($n = 4$). Statistical significance was assessed using one-tailed Student's *t* test. *n.s.*, not significant; *, $p < 0.05$.

firm that engraftment of a Gal binding footprint onto AAV2/AAV2i8 capsid templates increases transduction efficiency without altering the endogenous tissue tropism of these strains.

DISCUSSION

This study demonstrates that grafting conformational receptor footprints from one AAV strain onto another template is feasible. This strategy can clearly yield new chimeric AAV capsids with enhanced transduction profiles *in vitro* and *in vivo*. The overall approach was made possible by earlier reports that utilized molecular docking and alanine scanning mutagenesis to dissect structure-function correlates of AAV9-galactose interactions (13, 30). The dual glycan-binding chimera AAV2G9 was synthesized by incorporating residues from within or around the Gal binding pocket on AAV9 onto the AAV2 capsids. In addition, the Gal-binding AAV2i8G9 was constructed by deleting the partial HS footprint from AAV2G9. Remarkably, a minor change of nine residues in the primary amino acid sequence of the AAV2 VP3 subunit (~1.4%) was sufficient to impart Gal recognizing ability without affecting HS binding.

These results are particularly unique from a structural perspective. For instance, in the case of influenza A, mutations within a single sialic acid binding site have been associated with altered recognition of glycan linkage specificities by new reassortant strains (31, 32). However, it is noteworthy that the Gal- and HS-binding residues on AAV2G9 create two distinct and independent footprints on the viral capsid surface. Further, AAV2G9 appears to utilize HS and Gal simultaneously and interchangeably. On the other hand, the HS binding-deficient AAV2i8G9 strain is capable of engaging Gal alone to initiate transduction. Overall, this study sheds light on the modularity of the cluster of residues that form the "G9′" motif on the AAV9 capsid. On the basis of a similar rationale, our studies might provide design parameters for synthesizing a panel of orthogonal, dual, or perhaps even multiglycan receptor-binding AAV strains that might display enhanced transduction profiles.

Our results also provide insights into the biology of AAV receptor use *in vivo*. First, the tissue tropism of AAV2G9 and 2i8G9 *in vivo* appears to be dictated by one of the parental AAV serotypes, which composes a majority of the capsid structure. Specifically, AAV2G9 remains predominantly liver-tropic, like AAV2, whereas AAV2i8G9 is liver-detargeted, like the laboratory-derived AAV2i8 strain described earlier (15). This implies that utilization of the Gal receptor by AAV2G9/AAV2i8G9 is compatible with coreceptors such as fibroblast growth factor receptor, hepatocyte growth factor receptor, and/or integrins known to play a role in AAV2 cell entry (3, 4). Further, because Gal binding does not alter tissue tropism, it is tempting to speculate that the HS binding property of AAV2 is the primary determinant of liver tropism for this serotype. One question that follows this observation is whether incorporation of other glycan-binding footprints onto AAV2 or other serotypes (*e.g.*

Sia) will yield viable chimeric strains. Consequently, whether incorporation of other orthogonal glycan-binding footprints will enhance transduction and/or alter tropism remains to be seen. Nevertheless, such studies will likely shed more light on the specific role(s) played by different cognate glycan receptors in determining the tissue tropisms of different AAV serotypes.

We are currently examining the mechanism by which orthogonal Gal binding footprints enhance transduction efficiency *in vitro* and *in vivo*. Preliminary studies with galactose-overexpressing CHO-Lec2 cells suggest that the dual glycan-binding AAV2G9 strain binds more efficiently to the cell surface. This observation can be attributed to increased binding avidity to cell surface glycans. As a consequence, dual glycan-binding strains might show increased cellular uptake. Another aspect being explored is whether intracellular trafficking of dual glycan-binding strains follows alternative pathways that are consistent with HS or Gal receptor-mediated cell entry. Another potential scenario is the exploitation of a novel intracellular pathway(s) by chimeric strains that requires simultaneous engagement of HS and Gal moieties on the cell surface. Regardless of the outcome, such mechanistic studies are likely to help understand and possibly manipulate the interplay between host glycans and AAV serotypes.

For the gene therapy community, the new technology reported here provides a platform to develop improved clinical reagents. The orthogonal Gal-binding footprint clearly initiates earlier transgene expression that continues to increase at a faster rate compared with the less efficient parental AAV serotype. Although the transduction efficiencies of either chimeric strain did not surpass AAV9, the endogenous tissue tropisms of AAV2G9 and AAV2i8G9 (*i.e.* liver and muscle, respectively) remain unaltered. For instance, AAV2i8G9 is a one-of-a-kind, chimeric strain that can potentially serve as a vector candidate for selective gene transfer to cardiac and musculoskeletal tissue through intravenous infusion. Specifically, the selective muscle tropism and ability to avoid liver sequestration makes AAV2i8G9 an optimal vector for systemic gene therapy of muscular dystrophies (33–35). We determined recently that the strain described previously, AAV2i8, yields sustained transgene expression levels in primate muscle tissue[3]. Similar validation of AAV2i8G9 vectors in large animal models is forthcoming and will hopefully provide an attractive candidate for advancing toward the gene therapy clinic.

From a continued vector development standpoint, whether our new vector-engineering approach can be integrated synergistically with other major advancements in AAV technology (*e.g.* self-complementary vectors (36) or Tyr-to-Phe capsid mutations (37)) remains to be seen. The ultimate goal of such efforts is to continue to improve AAV vector technology that would help decrease the effective vector dose required for achieving therapeutically relevant transgene expression levels. These technological advancements are also likely to help alleviate potential clinical concerns associated with vector dose-dependent toxicity (38, 39). In summary, rational engineering of capsid-glycan receptor interactions is a promising approach toward continued improvement of the preclinical/clinical pipeline of AAV vectors for gene therapy. Improved structural understanding and manipulation of receptor-binding footprints on different AAV isolates as well as other closely related parvoviruses could help to further expand the AAV vector toolkit.

[3] A. Asokan, R. J. Samulski, and A. Tarantal, unpublished observations.

REFERENCES

1. Olofsson, S., and Bergström, T. (2005) Glycoconjugate glycans as viral receptors. *Ann. Med.* **37,** 154–172
2. Neu, U., Bauer, J., and Stehle, T. (2011) Viruses and sialic acids. Rules of engagement. *Curr. Opin. Struct. Biol.* **21,** 610–618
3. Agbandje-McKenna, M., and Kleinschmidt, J. (2011) AAV capsid structure and cell interactions. *Methods Mol. Biol.* **807,** 47–92
4. Asokan, A., Schaffer, D. V., and Samulski, R. J. (2012) The AAV vector toolkit: Poised at the clinical crossroads. *Mol. Ther.* **20,** 699–708
5. Halbert, C. L., Allen, J. M., and Miller, A. D. (2001) Adeno-associated virus type 6 (AAV6) vectors mediate efficient transduction of airway epithelial cells in mouse lungs compared to that of AAV2 vectors. *J. Virol.* **75,** 6615–6624
6. Wu, Z., Asokan, A., Grieger, J. C., Govindasamy, L., Agbandje-McKenna, M., and Samulski, R. J. (2006) Single amino acid changes can influence titer, heparin binding, and tissue tropism in different adeno-associated virus serotypes. *J. Virol.* **80,** 11393–11397
7. Ng, R., Govindasamy, L., Gurda, B. L., McKenna, R., Kozyreva, O. G., Samulski, R. J., Parent, K. N., Baker, T. S., and Agbandje-McKenna, M. (2010) Structural characterization of the dual glycan binding adeno-associated virus serotype 6. *J. Virol.* **84,** 12945–12957
8. Xie, Q., Lerch, T. F., Meyer, N. L., and Chapman, M. S. (2011) Structure-function analysis of receptor-binding in adeno-associated virus serotype 6 (AAV-6). *Virology* **420,** 10–19
9. Lerch, T. F., and Chapman, M. S. (2012) Identification of the heparin binding site on adeno-associated virus serotype 3B (AAV-3B). *Virology* **423,** 6–13
10. Opie, S. R., Warrington, K. H., Jr, Agbandje-McKenna, M., Zolotukhin, S., and Muzyczka, N. (2003) Identification of amino acid residues in the capsid proteins of adeno-associated virus type 2 that contribute to heparan sulfate proteoglycan binding. *J. Virol.* **77,** 6995–7006
11. Levy, H. C., Bowman, V. D., Govindasamy, L., McKenna, R., Nash, K., Warrington, K., Chen, W., Muzyczka, N., Yan, X., Baker, T. S., and Agbandje-McKenna, M. (2009) Heparin binding induces conformational changes in adeno-associated virus serotype 2. *J. Struct. Biol.* **165,** 146–156
12. O'Donnell, J., Taylor, K. A., and Chapman, M. S. (2009) Adeno-associated virus-2 and its primary cellular receptor. Cryo-EM structure of a heparin complex. *Virology* **385,** 434–443
13. Bell, C. L., Gurda, B. L., Van Vliet, K., Agbandje-McKenna, M., and Wilson, J. M. (2012) Identification of the galactose binding domain of the AAV9 capsid. *J. Virol.* **86,** 7326–7333
14. Xie, Q., Bu, W., Bhatia, S., Hare, J., Somasundaram, T., Azzi, A., and Chapman, M. S. (2002) The atomic structure of adeno-associated virus (AAV-2), a vector for human gene therapy. *Proc. Natl. Acad. Sci. U.S.A.* **99,** 10405–10410
15. DiMattia, M. A., Nam, H. J., Van Vliet, K., Mitchell, M., Bennett, A., Gurda, B. L., McKenna, R., Olson, N. H., Sinkovits, R. S., Potter, M., Byrne, B. J., Aslanidi, G., Zolotukhin, S., Muzyczka, N., Baker, T. S., and Agbandje-McKenna, M. (2012) Structural insight into the unique properties of adeno-associated virus serotype 9. *J. Virol.* **86,** 6947–6958
16. Arnold, K., Bordoli, L., Kopp, J., and Schwede, T. (2006) The SWISS-MODEL workspace. A web-based environment for protein structure homology modelling. *Bioinformatics* **22,** 195–201
17. Carrillo-Tripp, M., Shepherd, C. M., Borelli, I. A., Venkataraman, S., Lander, G., Natarajan, P., Johnson, J. E., Brooks, C. L.,3rd, and Reddy, V. S. (2009) VIPERdb2. An enhanced and web API enabled relational database for structural virology. *Nucleic Acids Res.* **37,** D436-D442
18. Kern, A., Schmidt, K., Leder, C., Müller, O. J., Wobus, C. E., Bettinger, K., Von der Lieth, C. W., King, J. A., and Kleinschmidt, J. A. (2003) Identification of a heparin-binding motif on adeno-associated virus type 2 cap-

sids. *J. Virol.* **77,** 11072–11081
19. Asokan, A., Conway, J. C., Phillips, J. L., Li, C., Hegge, J., Sinnott, R., Yadav, S., DiPrimio, N., Nam, H. J., Agbandje-McKenna, M., McPhee, S., Wolff, J., and Samulski, R. J. (2010) Reengineering a receptor footprint of adeno-associated virus enables selective and systemic gene transfer to muscle. *Nat. Biotechnol.* **28,** 79–82
20. Grieger, J. C., Choi, V. W., and Samulski, R. J. (2006) Production and characterization of adeno-associated viral vectors. *Nat. Protoc.* **1,** 1412–1428
21. Maheshri, N., Koerber, J. T., Kaspar, B. K., and Schaffer, D. V. (2006) Directed evolution of adeno-associated virus yields enhanced gene delivery vectors. *Nat. Biotechnol.* **24,** 198–204
22. Deutscher, S. L., and Hirschberg, C. B. (1986) Mechanism of galactosylation in the Golgi apparatus. A Chinese hamster ovary cell mutant deficient in translocation of UDP-galactose across Golgi vesicle membranes. *J. Biol. Chem.* **261,** 96–100
23. Shen, S., Bryant, K., Sun, J., Brown, S., Troupes, A., Pulicherla, N., and Asokan, A. (2012) Glycan binding avidity determines the systemic fate of adeno-associated virus 9. *J. Virol.* **86,** 10408–10417
24. Shen, S., Bryant, K. D., Brown, S. M., Randell, S. H., and Asokan, A. (2011) Terminal N-linked galactose is the primary receptor for adeno-associated virus 9. *J. Biol. Chem.* **286,** 13532–13540
25. Summerford, C., and Samulski, R. J. (1998) Membrane-associated heparan sulfate proteoglycan is a receptor for adeno-associated virus type 2 virions. *J. Virol.* **72,** 1438–1445
26. Bell, C. L., Vandenberghe, L. H., Bell, P., Limberis, M. P., Gao, G. P., Van Vliet, K., Agbandje-McKenna, M., and Wilson, J. M. (2011) The AAV9 receptor and its modification to improve *in vivo* lung gene transfer in mice. *J. Clin. Invest.* **121,** 2427–2435
27. Gao, G. P., Alvira, M. R., Wang, L., Calcedo, R., Johnston, J., and Wilson, J. M. (2002) Novel adeno-associated viruses from rhesus monkeys as vectors for human gene therapy. *Proc. Natl. Acad. Sci. U.S.A.* **99,** 11854–11859
28. Inagaki, K., Fuess, S., Storm, T. A., Gibson, G. A., Mctiernan, C. F., Kay, M. A., and Nakai, H. (2006) Robust systemic transduction with AAV9 vectors in mice. Efficient global cardiac gene transfer superior to that of AAV8. *Mol. Ther.* **14,** 45–53
29. Zincarelli, C., Soltys, S., Rengo, G., and Rabinowitz, J. E. (2008) Analysis of AAV serotypes 1–9 mediated gene expression and tropism in mice after systemic injection. *Mol. Ther.* **16,** 1073–1080
30. Adachi, K., Enoki, T., Kawano, Y., and Nakai, H. (2012) 15th Annual Meeting of American Society of Gene and Cell Therapy, Philadelphia, May 15–19, 2012, pp. S4–S5, Abstract 10, Molecular Therapy, Philadelphia, PA
31. Imai, M., Watanabe, T., Hatta, M., Das, S. C., Ozawa, M., Shinya, K., Zhong, G., Hanson, A., Katsura, H., Watanabe, S., Li, C., Kawakami, E., Yamada, S., Kiso, M., Suzuki, Y., Maher, E. A., Neumann, G., and Kawaoka, Y. (2012) Experimental adaptation of an influenza H5 HA confers respiratory droplet transmission to a reassortant H5 HA/H1N1 virus in ferrets. *Nature* **486,** 420–428
32. Herfst, S., Schrauwen, E. J., Linster, M., Chutinimitkul, S., de Wit, E., Munster, V. J., Sorrell, E. M., Bestebroer, T. M., Burke, D. F., Smith, D. J., Rimmelzwaan, G. F., Osterhaus, A. D., and Fouchier, R. A. (2012) Airborne transmission of influenza A/H5N1 virus between ferrets. *Science* **336,** 1534–1541
33. Kornegay, J. N., Li, J., Bogan, J. R., Bogan, D. J., Chen, C., Zheng, H., Wang, B., Qiao, C., Howard, J. F., Jr, and Xiao, X. (2010) Widespread muscle expression of an AAV9 human mini-dystrophin vector after intravenous injection in neonatal dystrophin-deficient dogs. *Mol. Ther.* **18,** 1501–1508
34. Fan, Z., Kocis, K., Valley, R., Howard, J. F., Chopra, M., An, H., Lin, W., Muenzer, J., and Powers, W. (2012) Safety and feasibility of high-pressure transvenous limb perfusion with 0.9% saline in human muscular dystrophy. *Mol. Ther.* **20,** 456–461
35. Bowles, D. E., McPhee, S. W., Li, C., Gray, S. J., Samulski, J. J., Camp, A. S., Li, J., Wang, B., Monahan, P. E., Rabinowitz, J. E., Grieger, J. C., Govindasamy, L., Agbandje-McKenna, M., Xiao, X., and Samulski, R. J. (2012) Phase 1 gene therapy for Duchenne muscular dystrophy using a translational optimized AAV vector. *Mol. Ther.* **20,** 443–455
36. McCarty, D. M. (2008) Self-complementary AAV vectors. Advances and applications. *Mol. Ther.* **16,** 1648–1656
37. Zhong, L., Li, B., Mah, C. S., Govindasamy, L., Agbandje-McKenna, M., Cooper, M., Herzog, R. W., Zolotukhin, I., Warrington, K. H., Jr, Weigel-Van Aken, K. A., Hobbs, J. A., Zolotukhin, S., Muzyczka, N., and Srivastava, A. (2008) Next generation of adeno-associated virus 2 vectors. Point mutations in tyrosines lead to high-efficiency transduction at lower doses. *Proc. Natl. Acad. Sci. U.S.A.* **105,** 7827–7832
38. High, K. A. (2012) The gene therapy journey for hemophilia. Are we there yet? *Blood* **120,** 4482–4487
39. Mingozzi, F., and High, K. A. (2011) Therapeutic *in vivo* gene transfer for genetic disease using AAV. Progress and challenges. *Nat. Rev. Genet.* **12,** 341–355